Phase transformations of 4,4′-biphenyldicarboxylic acid on Cu(001)

Daniel Schwarz, Raoul van Gastel, Harold J. W. Zandvliet, and Bene Poelsema
Physics of Interfaces and Nanomaterials, MESA + Institute for Nanotechnology, University of Twente, P.O. Box 217, NL-7500AE Enschede, The Netherlands

(Received 22 February 2012; revised manuscript received 10 May 2012; published 7 June 2012)

The growth and structure of 4,4′-biphenyldicarboxylic-acid (BDA) on Cu(001) at temperatures between 300 and 400 K was studied by low energy electron microscopy and μ-LEED. First, the adsorbed BDA molecules form a disordered dilute phase. Once this phase reaches a sufficiently high density, a crystalline phase nucleates, in which the molecules form a hydrogen-bonded two-dimensional (2D) supramolecular $c(8 \times 8)$ network. By a careful analysis of the bright-field image intensity, we can measure the density in the dilute phase, which is up to 30% of that in the crystalline phase. From the respective equilibrium densities at different temperatures, we determine the 2D phase diagram and extract a cohesive energy of 0.35 eV. We also analyze the island decay behavior and estimate the BDA molecule diffusion constants. Steps are found to be highly transparent for diffusing BDA molecules. In the temperature range of 362–400 K, we find chemical diffusion constants between 850–1700 $nm^2\,s^{-1}$.

DOI: 10.1103/PhysRevB.85.235419 PACS number(s): 68.43.Jk, 68.37.Nq, 68.35.Rh, 68.55.−a

I. INTRODUCTION

The self-assembly of organic molecules into large supramolecular networks is a promising method for the fabrication of novel nanoscale structures.[1–4] Hydrogen bonds, which can be highly selective, play an important role in the self-assembly process. One of the more frequently studied building blocks are benzoic acid groups.[5–12] It has been reported that benzoic acids adsorb on Cu(001) as deprotonated carboxylate species.[5–7] 4,4′-biphenyldicarboxylic-acid (BDA) is an organic molecule with two phenyl rings and two functional carboxyl end groups. It is a nonchiral molecule that is 1.3 nm in length (see Fig. 1). On Cu(001), the molecules adsorb in a flat-lying configuration. Reevaporation (or desorption) into vacuum does not occur; the molecules decompose on the surface above 450 K. Below these temperatures, BDA exists in two phases on Cu(001): a dilute phase and a two-dimensional (2D) crystalline phase which nucleates from the dilute phase.[9] In the crystalline phase, the molecules form a well-ordered, square network with a $c(8 \times 8)$ superstructure, as was found by scanning tunneling microscopy (STM) and μ-LEED.[8,9] An example of the μ-diffraction pattern obtained from the structure is shown in Fig. 2. Adjacent molecules are rotated by 90 degrees and the lateral molecule-molecule interaction is governed by hydrogen bonds formed between the phenyl rings of one molecule and the carboxylate end group of the next molecule (see Fig. 1).

Calculations show that the two benzene rings constituting the single BDA molecule are twisted along the long axis of the molecule in vacuum. While for BDA adsorbed on, e.g., Au(111) both rings are expected to be in-plane,[10] we found in a previous μ-LEED study that they are also twisted on Cu(001).[9]

The strength of the molecule-molecule interaction as well as the diffusion constant are key ingredients to understand and control the self-assembly process and important input parameters for simulations. However, they are difficult quantities to access experimentally. It is also not clear how the underlying substrate influences the interaction strength. In this paper, we will show how low energy electron microscopy (LEEM) can be used to measure the density in the disordered phase by analyzing the local electron reflectivity. This allows us to construct a 2D phase diagram, which provides a direct route to determine the cohesive energy of a molecule in the 2D network. Additionally, we will study the decay of the domains using the measured mean densities in the dilute phase.

II. EXPERIMENT

Experiments were performed in an Elmitec LEEM III low energy electron microscope with a base pressure of about 1×10^{-10} mbar. A Cu(001) single crystal with a miscut angle of less than 0.1 degrees was used.[13] To deplete the bulk of the crystal from impurities like carbon and, especially, sulfur, it was annealed at 1173 K under a flow of an Ar-H_2 gas at atmospheric pressure for 48 h. After transferring the crystal to the LEEM, the surface was further cleaned by cycles of sputtering with atomic hydrogen,[14] sputtering with argon ions, and annealing at 900 K. This method allowed us to prepare clean surfaces with sharp LEED spots, large terraces, and smooth step lines.

Commercially available BDA in powder form (purity >97%, TCI europe, CAS: 787-70-2) was deposited from a Knudsen-cell-type source. Before the experiments, the BDA source was carefully degassed. Throughout the experiments, the source was held at one of two temperatures. The corresponding deposition rates differ by a factor of ~ 4. During deposition, the Cu(001) surface was held at constant temperatures between 300 and 420 K.

A 25-μm illumination aperture was used to limit the illuminated area on the surface. Any potential influence of the electron beam on the BDA behavior, e.g., differences in island size distribution and nucleation density, would therefore become visible at the edge of the illuminated area, which was never observed under the imaging conditions selected here.

Images in bright field mode were taken by selecting the (00) LEED spot using a contrast aperture. All images were background corrected by applying a flat field correction using a mirror mode image taken before the experiments. In this way we are able to correct for any inhomogeneous illumination and inhomogeneities of the MCP detector. This procedure proved to be very reliable in removing intensity gradients allowing

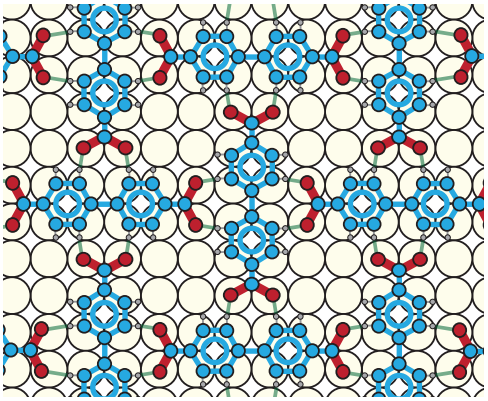

FIG. 1. (Color online) Schematic arrangement of the BDA molecules in the $c(8 \times 8)$ domains on Cu(001). The blue (light gray), red (dark gray), and smaller gray dots represent C atoms, O atoms, and H atoms, respectively.

the comparison of intensity data from different parts of the images. In the μ-LEED pattern shown in Fig. 2(b), additionally a cloud of secondary electrons in the lower left part was removed. The secondary electrons yield only little information, but usually obscure the diffraction spots. To remove them, a background image was generated from the original LEED pattern in Fig. 2(a) by applying three simple filters. First an erosion filter leaves only the minimum intensity value in a radius of 20 pixels, followed by the inverse operation using a dilation filter. By applying these operations, the intensity in the diffraction spots is almost completely removed and only the intensity from the secondary electron cloud remains. Finally, a Gaussian filter is used to smooth the generated background. Each pixel of the original LEED pattern is then divided by the corresponding pixel in the background. This procedure allows us to increase the contrast dramatically without having the secondary electron cloud obscuring half of the diffraction pattern.

III. MEASUREMENT OF THE DENSITY IN THE DILUTE PHASE

A. BDA-induced change of electron reflectivity

The measurement of the density in a dilute 2D surface phase by the attenuation of a scattering beam is a well known technique. For example, He scattering was used to measure the 2D gas to 2D gas + 2D solid transition of Xe on Pt(111).[15–18] Recently, the technique was also applied in LEEM, where the real-space image helps in distinguishing between a solid/liquid and disordered phase. Examples are the growth of Ag on W(110) (Ref. 19) and C on Ru(0001) and Ir(111).[20,21] In LEEM, a dilute or 2D gas phase leads to a decrease in image intensity of the substrate terraces. In previous LEEM studies, this resulted in a drop of image intensity that is proportional to the local adatom concentration. The sensitivity of this method is up to 10^{-3} ML, depending on the system investigated.[19]

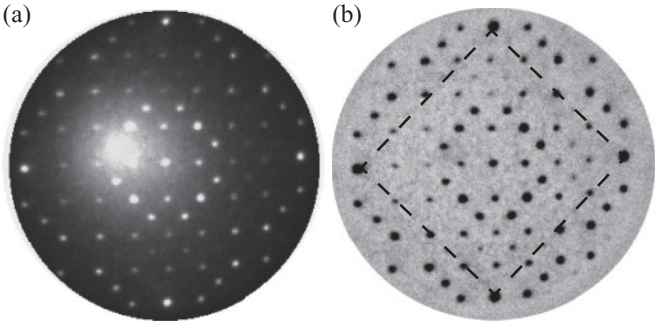

FIG. 2. μ-LEED pattern of the BDA domains measured at an electron energy of 27 eV. The dashed lines connect the Cu(001) first-order spots. (a) Measured and (b) background corrected pattern.

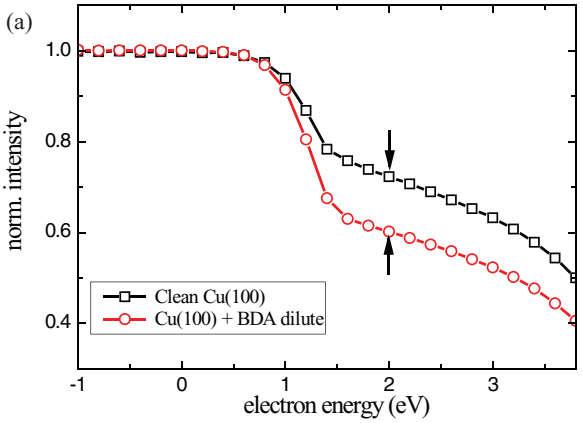

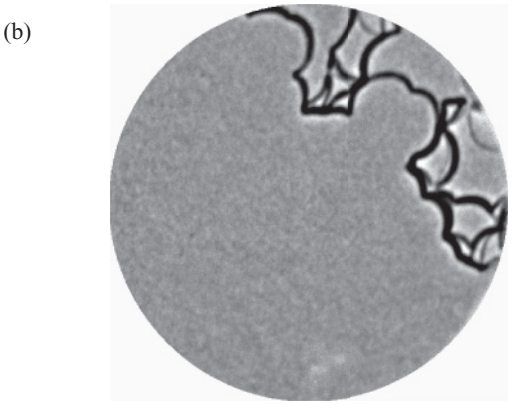

FIG. 3. (Color online) (a) LEEM IV curves measured on a clean Cu(001) terrace and on a terrace covered with BDA in the dilute phase. The BDA coverage is approximately 0.01 ML, expressed in occupied Cu lattice sites. Arrows indicate the energy used for imaging, 2 eV. (b) LEEM image of a large Cu terrace with BDA gas [field of view (FOV) 4 μm]. The molecules give rise to a homogeneous decrease of the image intensity. No density gradients can be observed. The lighter area in the lower part of the image is due to a defect in the MCP detector.

To have maximum sensitivity, it is necessary to know how the BDA in the dilute phase changes the electron reflectivity of the Cu(001) surface. Figure 3(a) shows LEEM-IV curves for the clean Cu(001) surface and for the surface covered with BDA molecules in the dilute phase at a coverage before island nucleation (see the LEEM image in Fig. 3). Both curves were normalized to the intensity at negative energy <0 eV. In the region between 1.5 and 3.5 eV, the relative difference between the curves is largest. We used an electron energy of 2 eV for further imaging. No density gradients can be observed, close to a BDA domain or on different Cu terraces. The BDA molecules

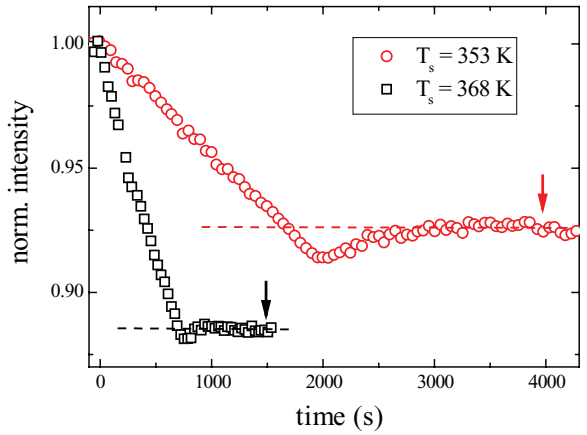

FIG. 4. (Color online) Normalized intensity change measured on the Cu terrace (far away from spots where BDA domains eventually nucleate) during deposition of BDA at 353 and 368 K. After the shutter is opened, the intensity drops linearly until BDA islands nucleate at 750 s (368 K) and 2000 s (353 K), respectively. The two curves were obtained at different deposition rates. We verified that the initial slope of the decay curves at a fixed deposition rate does not depend on the substrate temperature. The shutter is closed at $t = 3900$ s (353 K) and $t = 1500$ s (368 K), respectively (arrows).

in the 2D dilute phase give rise to a homogeneous change in intensity covering all parts of the surface.

Next, we need to understand this intensity change as a function of coverage. For this we tracked the bright field intensity of the Cu terraces for different conditions at an electron energy of 2 eV while depositing molecules. In Fig. 4, we show the evolution of the intensity of two representative experiments. The experiments were done with deposition rates, which differ by about a factor of 4, as well as with different substrate temperatures (353 and 368 K, respectively). We emphasize that the initial slope of such an uptake curve (electron reflectivity versus deposition) only depends on deposition rate and not on the substrate temperature. At $t = 0$ s, the shutter of the source is opened and the intensities are normalized to this point. After opening the shutter, the normalized intensities $\frac{I}{I_0}$ start to drop linearly with time. The slope depends on the source temperature; the higher setting leads to a larger slope. The change in intensity is proportional to the density of molecules on the surface. At $t = 750$ s (black circles) and 2000 s (red squares), BDA domains start to nucleate from the dilute phase. The domains mainly nucleate on the Cu terraces (homonucleation) and are blocked in their growth by both upward and downward Cu steps (see Fig. 5). The nucleation is accompanied by a sharp transition in the intensity on the terraces. Because of the nucleation barrier, the dilute phase was supersaturated during nucleation.[22] This results in an increase of intensity after nucleation when BDA domains grow not only from the molecules that arrive from the evaporator, but also at the expense of the supersaturation on the "bare" terraces. After some minutes, the intensity stabilizes at a constant value, which means that a dynamic equilibrium is reached. This value is also close to the true equilibrium, and thus low supersaturation, since no change in intensity is observed when the shutter is closed at $t = 3900$ s (353 K) and $t = 1500$ s (368 K).

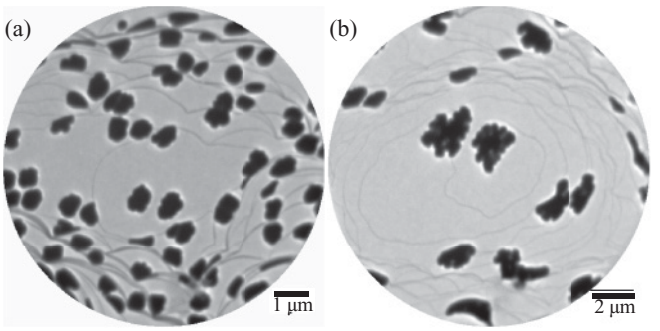

FIG. 5. LEEM images corresponding to the experiment in Fig. 4. The images show the island configuration at the end of the deposition for (a) 353 K and (b) 368 K. By averaging several images at different positions, we find that the islands cover 11% (a) and 10% (b) of the surface.

Due to the statistical overlap of the diffuse scattering cross section of individual scatterers, the intensity should in principle decay exponentially.[16–18] The slope is given by

$$d(I/I_0)/dt = -\Sigma \exp(-\Sigma n) dn/dt, \tag{1}$$

where Σ is the BDA scattering cross section and n is the BDA density. Since in this case we are covering only small Σn values up to 0.15, the exponential behavior is approximated well by a linear uptake curve. In the crystalline phase, each molecule covers an area of 1.04 nm^2 and the corresponding density is therefore 0.96 nm^{-2} or one molecule per 16 Cu atoms. For the remainder of the article, we will express coverage (or density) as the fraction of occupied Cu-lattice sites. A closed $c(8 \times 8)$ layer corresponds to a coverage of 0.0625 ML.

It is now straightforward to determine the cross section for diffuse scattering, Σ, introduced in Eq. (1). The final level of the normalized intensity in Fig. 4 is determined by the density of the dilute phase, n_d, corresponding to the 2D vapour, and Σ. This level has been reached first at time t_1, where all deposited molecules belong to the dilute phase. At the end of the experiment at time t_2 a fractional area A_c is covered with the condensed phase with a higher density $n_c = 0.0625$. Assuming that all molecules that hit the surface are incorporated in the film leads to the situation in which $n_d(A_c + t_2/t_1 - 1)$ molecules contribute to an area A_c with density n_c. The resulting value for n_d equals $0.0625A_c/(A_c + t_2/t_1 - 1)$. Consequently, $\Sigma = -\ln(I(t_2)/I_0)/n_d$, or $\Sigma \approx [1 - I(t_2)/I_0]/n_d$, with n_d being approximately an order of magnitude smaller than n_c for the data shown in Fig. 4. With $A_c = 0.11 \pm 0.01$ and 0.10 ± 0.02 for $T = 353$ and 368 K, respectively, the resulting mean value for $\Sigma = 1.2 \pm 0.1$ nm^2. In principle, Σ depends on the energy of the probing electrons and by coincidence the value at 2 eV is close to the actual area of the molecule. This implies that statistical overlap is negligible and we can, to a good approximation, use a linear relationship between intensity and density. The density in the dilute phase at time t is then given through the intensity $I(t)$ by

$$\theta_{\mathrm{BDA}}(t) = 0.052 \times \frac{I_0 - I(t)}{I_0}\ \mathrm{ML}, \tag{2}$$

where I_0 is the intensity when the shutter was opened at $t = 0$ s. A drift of the instrument (cathode emission current or

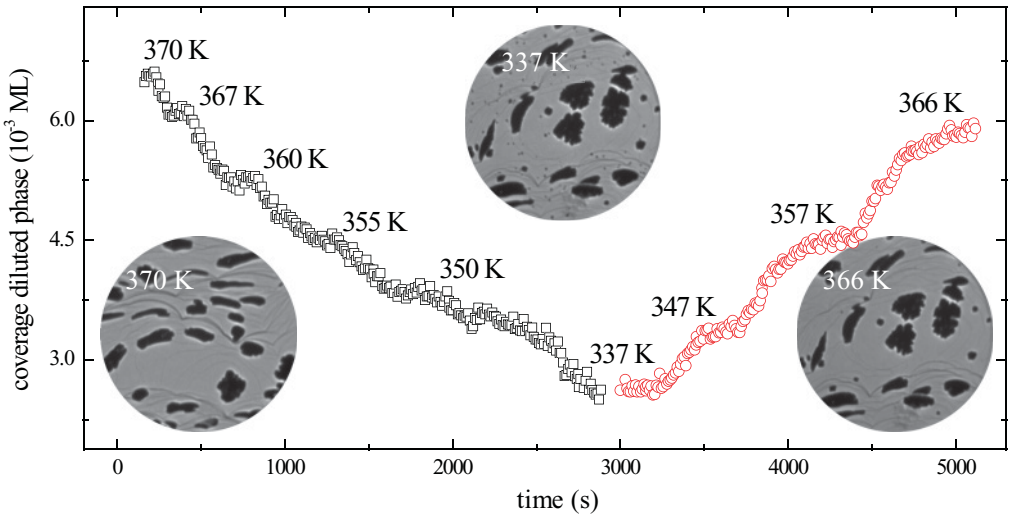

FIG. 6. (Color online) Experiment to determine the equilibrium BDA density in the dilute phase. First BDA domains were grown at 370 K. Then the sample was cooled in steps to 337 K. Next, the sample was heated again in three steps. The temperature of each step is indicated in the figure. Each temperature was maintained until the intensity was constant. LEEM images show the configuration at the start of the experiment (left) after cooling down (middle) and after heating again (right); 15 μm FOV.

alignment) will change this initial intensity and thus change the normalization. One might expect that the intensity of the BDA $c(8 \times 8)$ gives a possibility to normalize the intensity, however due to field distortion at the island's perimeter this intensity is not uniform and is decreasing toward the island center.

With this result we return to Fig. 4 for a moment. Nucleation occurs at coverages of about 4.5×10^{-3} ML (red curve, 353 K) and 6.3×10^{-3} ML (black curve, 368 K). Compared to values common in epitaxial growth of, e.g., metals, these values are very large. The relative densities in the dilute phase, corresponding to the 2D vapor pressure, are up to 30% of the crystalline structure. This fortunate fact allows us to monitor the density in the dilute phase in a relatively wide temperature window. The system is already close to equilibrium, i.e., in a low supersaturation stage, where the 2D dilute phase has a high density. After nucleation, the density goes down slightly, which means that the dilute phase was significantly supersaturated during the nucleation period. Supersaturation is genuinely necessary for nucleation due to the aforementioned nucleation barrier. For an ideal 2D gas, the supersaturation $\Delta\mu$ is defined as $\Delta\mu = k_B T \ln(\frac{\theta}{\theta_{eq}})$, where θ is the gas density.[22,23] The equilibrium density θ_{eq} is almost identical to the plateau reached at the end of both curves, 3.8×10^{-3} and 5.9×10^{-3} ML. Taking these numbers, we find maximum supersaturations of about 5 and 2 meV per molecule. These rather small values indicate that the system is only slightly out of equilibrium for nucleation to occur.

IV. PART I—BDA 2D PHASE DIAGRAM

In the preceding section, we determined the local molecule concentration in the dilute phase. We apply the same method now to determine the equilibrium density in the presence of large BDA domains in a temperature range from 330 to 420 K. BDA domains were grown at different temperatures in individual experiments on freshly cleaned substrates. After growing sufficiently large islands, the temperature was changed in discrete steps of about 5–10 K. At each step, the system was given time to reach equilibrium again. When the temperature is lowered, molecules in the dilute phase attach to existing BDA domains or nucleate to form new domains if the temperature change was too fast. Slowly a new constant density is reached and the system is in equilibrium again. We assume that the BDA islands merely act as a reservoir for molecules and have large enough curvature. The latter condition is necessary to avoid a size dependence of the equilibrium density, since domains with a small curvature will have a larger corresponding vapor pressure (Gibbs-Thomson relation). An example of such an experiment is shown in Fig. 6. Large BDA domains were grown at 370 K. Then the sample was cooled down in discrete steps to 337 K. Next the sample was heated again in three steps. The temperatures of each step are indicated in the figure. Each temperature was maintained until the intensity did not change anymore. The relatively long time before the density equilibrates, especially during the heating steps, shows that the molecular diffusion is rather slow. This will introduce a small error when the measured concentration is actually not yet the equilibrium value. In Fig. 7, we show the resulting 2D phase diagram, summarizing the data from several measurements. The data obtained for the equilibrium concentration after a temperature increase are denoted with top-up triangles and those obtained after a temperature decrease are denoted by top-down triangles. Data points derived directly from the isothermal deposition curves, shown in Fig. 4, are denoted with squares. It is obvious that the data points are probing identical situations, proving that they represent thermal equilibrium data. The measured equilibrium densities lie on a line that is closely following a logarithmic curve.

On the dividing line, the chemical potential of the dilute phase μ_d and the $c(8 \times 8)$ phase μ_s have to be equal, meaning that no net mass transport occurs from one phase to the other. Phenyl rings have a strong affinity with fourfold hollow sites

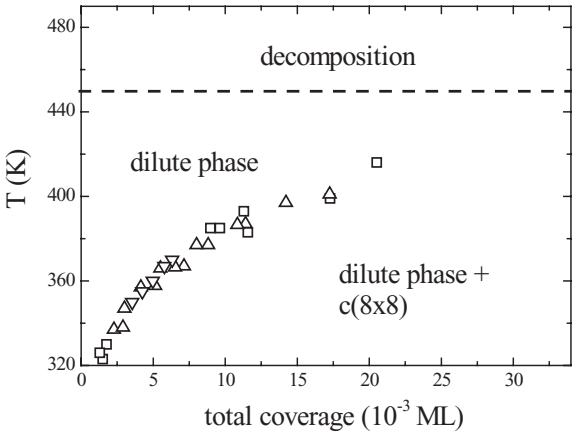

FIG. 7. 2D phase diagram of BDA on Cu(001). Copper-assisted decomposition of the molecules starts at temperatures above 450 K. Squares give the equilibrium density after growth (see Fig. 4), downward triangles represent cooling experiments, and upward triangles represent heating experiments (see Fig. 6).

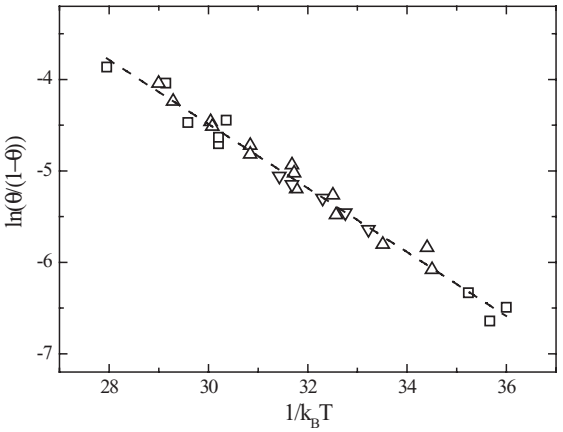

FIG. 8. Plot of $\ln(\frac{\theta}{1-\theta})$ vs $1/kT$ from Fig. 7. The data can be fitted with a straight line with a slope of 0.35 ± 0.03 eV. For the meaning of the symbols, see Fig. 7.

and threefold hollow sites on, respectively, fcc (100) and (111) surfaces.[24,25] This would lead to the $c(8 \times 8)$ structure as sketched in Fig. 1. We will have the occupation of these sites in mind also for the molecules in the dilute phase. We emphasize, however, that this assumption is irrelevant for our further considerations, which would apply also for bridge or on-top sites. The molecules will form a lattice gas where they are free to jump between different fourfold hollow lattice sites with a probability that is governed by the diffusion constant.[26–28] By equating the chemical potentials μ_d and μ_s, we can calculate the density in the dilute phase. Neglecting vibrational excitations and thus negating entropy in the crystalline phase, the chemical potential of an atom in the crystalline phase is equal to the (negative) cohesive energy ($\mu_s = -E_C$), the energy difference between a molecule in the solid and in the dilute phase. In the dilute phase, the chemical potential contains entropy terms and a coverage-dependent mean field interaction term $W(\theta)$:

$$\mu_d = k_B T \ln\left(\frac{\theta}{1-\theta}\right) - k_B T \ln(Z) + W(\theta). \qquad (3)$$

The first term follows from occupation statistics, and the second term, with Z representing the partition sum, summarizes the remaining entropy terms. The latter will contain, for example, vibrational or rotational terms. By equating μ_s and μ_d, we find

$$\frac{\theta}{1-\theta} = \exp\left(\frac{-E_C - W(\theta)}{k_B T} + \ln(Z)\right). \qquad (4)$$

Plotting $\ln(\frac{\theta}{1-\theta})$ versus $1/k_BT$ should therefore give a curve with a slope of $-E_C - W(\theta)$. This is done in Fig. 8. The data scatter along a straight line with a slope of 0.35 ± 0.03 eV and with an intersection with the ordinate at $\ln(Z) = 6.02$. Measurement errors arise mainly from small drifts of the total image brightness, which change the reference point of the intensity normalization. This is also limiting the resolution at low coverages (temperatures), where intensity changes of a few percent were tracked over up to half an hour.

A. Discussion on the cohesive energy

The slope in Fig. 8 gives us a value for $E_C + W(\theta)$. In the analysis, we cannot separate the cohesive energy from the mean field interaction term. Molecules will not only interact attractively through the short ranged hydrogen bonds, but also by exclusion of lattice sites and through repulsive long ranged Coulomb forces from the negatively charged carboxylate groups. This means that the sign and coverage dependence of $W(\theta)$ are unknown. The sign might even change with coverage. However, from the quality of the straight fit, we conclude that $W(\theta)$ has to be rather small. A larger value would introduce a coverage-dependent slope. A good estimate for the cohesive energy is therefore given by $E_C = 0.35 \pm 0.03$ eV.

From the temperature independent part in Fig. 8, we find an entropy term of $\ln(Z) = 6.02$. In a simple model, i.e., a monatomic lattice gas where every gas atom occupies exactly one site and has no vibrations, $\ln(Z)$ should be zero. However, the size and the structure of the molecules add entropy terms. These will contain, for example, rotational and vibrational terms which are frustrated in the crystalline phase. Also, a term that is introduced by blocking of neighboring sites through the molecules in the dilute phase contributes. In the $c(8 \times 8)$ phase, each molecule blocks 16 lattice sites (see Fig. 1), while in the dilute phase one molecule blocks on average 41 sites and possibly more if we take into account the repulsion from the negatively charged carboxylate groups (see Fig. 9). On the other hand, for larger densities the molecules will have to order, thereby reducing the number of occupied sites down to 16 in the limit of full coverage. This effect will change the configurational entropy for molecules in the dilute phase, also as a function of coverage.

The $\ln(Z)$ term increases the density in the dilute phase by a factor of Z compared to a monatomic lattice gas with the same cohesive energy. It is important to note that the large densities that we observe in the dilute phase, up to half of the density in the $c(8 \times 8)$, do not originate from a weak intermolecular interaction, but rather from the size and structure of the molecule.

The BDA molecules form a square 2D crystal with four nearest neighbors for each molecule. Hydrogen bonds are

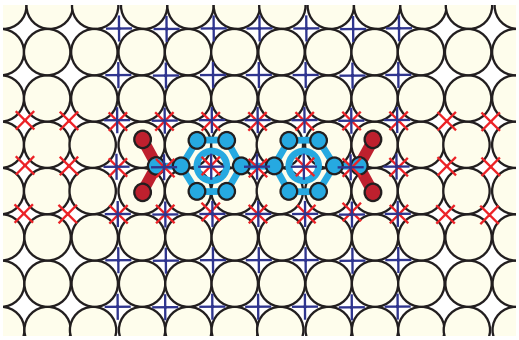

FIG. 9. (Color online) Sketch illustrating the number of Cu-lattice sites blocked by one molecule assuming a hard sphere model. The center of mass on a marked lattice site cannot be occupied by another molecule. Red crosses (33) are blocked for molecules oriented parallel; blue pluses (49) are blocked for perpendicular oriented molecules. With equal probability for parallel and perpendicular orientation, we arrive at a mean number of blocked sites of 41.

very short ranged, so we can assume that nearest neighbor interaction will be by far the largest contribution to the cohesive energy. Therefore, the cohesive energy is equal to the binding energy of a molecule in a kink position, which corresponds to a molecule with two nearest neighbors. This means that the strength of an individual bond between two molecules is $E_{\mathrm{NN}} = 0.175$ eV. The cohesive energy was determined for perylene-3,4,9,10-tetracarboxylic acid dianhydride (PTCDA) on Ag(100) in a more indirect way by fitting decay curves.[29] For this system, a somewhat lower value of 100 meV was found.

In the $c(8 \times 8)$ structure, each bond is made by hydrogen bonds from the carboxylate group of one molecule to the two nearest carbon atoms of both phenyl rings of the neighboring molecule. The hydrogen bonds are formed by the negatively charged oxygen atoms and the positively polarized hydrogen atoms of the phenyl rings. Since carbon is only slightly more electronegative than hydrogen, the polarization will be rather small, which limits the overall hydrogen bond strength. If we treat the bond as two independent C-H··O bonds, we find a dissociation energy of 0.09 eV for each bond. This value is well in the range expected for a weak hydrogen bond.[30] The hydrogen bond strength usually depends strongly on temperature and pressure due to changing bond lengths. However, here the BDA molecules are locked in position by the underlying substrate. Ignoring the small thermal expansion of the Cu substrate, the bond length will therefore remain constant and accordingly so will the binding strength.

From the value for the cohesive energy, we can estimate the line tension in a nearest neighbor model. In this model, the line tension per molecule is equal to one-quarter of the cohesive energy: $\gamma^* = 0.09 \pm 0.015$ eV. The actual value of the line tension will depend on the shape of the island, which can introduce a correction on the order of 10%.[31] We will use this value for γ^* in the next part to analyze BDA island decay, which allows us to estimate the molecule diffusion constant.

V. PART II—ISLAND DECAY

The decay kinetics of islands on a surface was studied extensively and allows us to obtain information on diffusion constants and boundary energies.[29,31–36] Here, we will first use a classical approach to analyze the decay of small islands. With the previously obtained information on the line tension γ^* and equilibrium densities $\theta_{\mathrm{eq}}(T)$, this allows us to estimate the diffusion constant.

Upon changing the substrate temperature, we change the equilibrium condition between the dilute and crystalline phase. This leads to mass transport toward or away from the islands, and islands grow or decay as can be seen in the insets in Fig. 6. The driving force for the growth or decay is the difference between the actual mean density $\overline{\theta}$ and the equilibrium density θ_r of the dilute phase. Generally, θ_r will depend on the island's curvature r according to the Gibbs-Thomson relation:

$$\theta_r = \theta_\infty \exp\left(\frac{\gamma\Omega}{kTr}\right), \tag{5}$$

where r is the island curvature, γ is the line tension, Ω is the area occupied by each molecule, and θ_∞ is the equilibrium density of an infinitely large island. The change of the island area A is then given by

$$dA/dt = -\kappa(r)(\theta_r - \overline{\theta}), \tag{6}$$

$$dA/dt = -\kappa(r)\left[\theta_\infty \exp\left(\frac{\gamma\Omega}{kTr}\right) - \overline{\theta}\right], \tag{7}$$

where $\kappa(r)$ is a rate constant that contains the diffusion constant and geometry information. The decay can either be limited by the rate at which molecules diffuse away from the islands or by the detachment of molecules from the island.[37–40] In the case of diffusion limited decay, the rate constant is given by $\kappa_D = \frac{2\pi\Omega D(T)}{l_c}$. $D(T)$ is the temperature dependent diffusion constant and l_c is a screening length. Typically the expression $l_c = \ln(R/r)$ is used for the screening length, where r is the islands' radius and R is the distance away from the islands' edge where θ_∞ is reached. This expression is exactly valid only for a concentric geometry, e.g., an isolated island on a large terrace. Compared to the exponential term in Eq. (7), it is changing only slowly with r and is typically approximated to be a constant on the order of 1. Analytical solutions for l_c exist only for a few special geometries.[34]

A. Decay of small islands—Classical Ostwald theory

In a previous study, we showed indications for a diffusion limited BDA island decay.[9] Diffusion limited decay was also found in a similar system, namely PTCDA on Ag(100).[29] In the classical Ostwald theory, Eq. (7) is integrated using a first-order approximation of the Gibbs-Thomson term and assuming that the surrounding mean density is equal to θ_∞.[33,37,39] It follows that the island area decreases like $\alpha(t_c - t)^{2/3}$ for diffusion limited decay. It is straightforward to find an expression for α in this case:

$$\alpha = \pi\left(3\frac{\Omega^2\theta_\infty\gamma D(T)}{l_c k_B T}\right)^{2/3}. \tag{8}$$

Figure 10 shows five decay curves of neighboring BDA islands. The temperature was increased in one step from 348 to 362 K starting at $t = 2500$ s and reached the final temperature at about $t = 3000$ s. We can see that individual decay curves

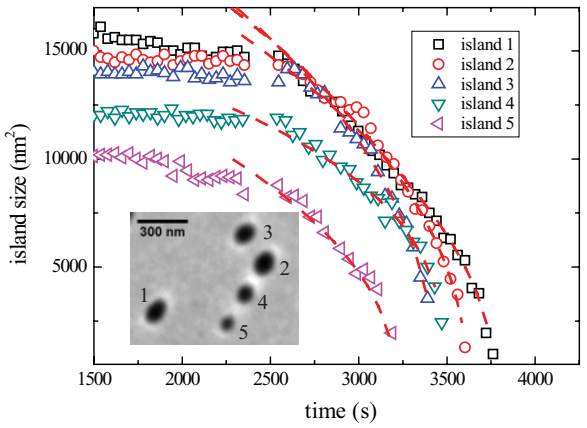

FIG. 10. (Color online) Size evolution of decaying islands at 362 K, shown in the inset. The temperature was changed from 348 K at about 2500 s and reached the final value of 362 K at about 3000 s. The red dashed lines are fits of the type $\alpha(t_c - t)^p$ with exponents between 0.35 and 0.53 and prefactors α of 400–950 nm^2 s$^{-2/3}$. Only the last part of the curves was used for fitting where the temperature change was negligible.

cross each other several times, for example island 3 and 4 at $t = 3400$ s. This cannot be understood within the simple model. Local correlations influence the decay behavior of individual islands. This is a feature of diffusion limited decay, where the exact arrangement of islands determines the decay rate through density fields. Nevertheless, the final parts of the decay curves, where the temperature change was negligible, could be fitted with curves of the form $\alpha(t_c - t)^p$. The fitted exponents p are between 0.35 (island 5) and 0.53 (island 1) and prefactors α are approximately 400 nm^2 s$^{-2/3}$. The exception is island 3, which decays much faster and has a prefactor of 950 nm^2 s$^{-2/3}$. The exponents that we find are smaller than the 2/3 expected from diffusion limited decay, but are clearly incompatible with the exponent of 1 expected for interface limited decay. Smaller exponents are expected if the linearization of the Gibbs-Thomson term in Eq. (7) is not justified, i.e., $\frac{\gamma\Omega}{kTr}$ is large. From the presence of local correlations in the decay process and critical exponents well below 1, we conclude that the decay is indeed, at least partially, limited by diffusion. However, we cannot exclude a mixed case, i.e., also the detachment of molecules is an important factor in the decay.

The classical Ostwald theory approach that we used here has two major deficiencies: First, it does not include the local correlations between the decaying islands, which we observe. Secondly, it assumes a constant mean density $\overline{\theta}$, implying that the decay is only driven through the size dependence of θ_r. This is a crude approximation since the decay involves large amounts of molecules transported from the islands into the dilute phase changing $\overline{\theta}$.

Since we are able to measure $\overline{\theta}$ and we know the equilibrium density, we can, in principle, fit the curves with Eq. (7) directly. However, this will fail for the rather small islands in Fig. 10. We cannot resolve $\overline{\theta}$ locally. Figure 11 shows a LEEM image of the islands from Fig. 10 at $t = 3250$ s. In the right hand image of that figure, the color scale was scaled to represent the molecule density. No gradients can be observed between

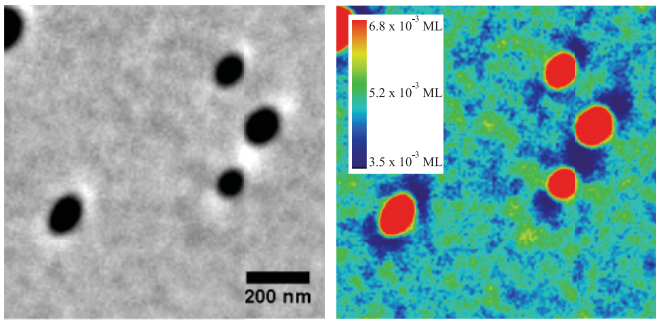

FIG. 11. (Color online) Left: LEEM image of the BDA domains in Fig. 10 at $t = 3250$ s. Right: The same image in false colors representing the molecular density between the islands. The high contrast makes the island appear bigger. The blue areas around the islands going from bottom left to top right are due to lensing effects (see text), obscuring density gradients close to the islands edges.

the islands. Unfortunately, work function differences between BDA and Cu lead to lensing effects (blue halos around the islands),[41] which hide the particularly interesting molecular density close to the islands' edges. The density should drop fast from island edges, while further away the change becomes considerably smaller.[33] For most of the decay in Fig. 10, the islands are larger than 2500 nm^2. A quick estimate of the vapor pressure of such an island using Eq. (5) gives a value that is ∼11% above the equilibrium density. This would be the maximum density change from the edge of an island of such size to sufficiently far away. A density difference of this size would be of the order of the noise level in Fig. 11 and is thus not detectable under the conditions here.

B. Decay of large islands

To avoid the local correlations, we will now analyze the decay of large, well separated islands. Figure 12 shows a LEEM image of the relevant islands. The initial island sizes were between 6×10^5 and 1.4×10^6 nm^2, with cauliflower-like shapes. This is not the equilibrium shape. We observed that the islands become compact on a time scale of several hours. In the experiment, the temperature was changed in two steps, first from 375 to 386 K and then from 386 to 400 K.

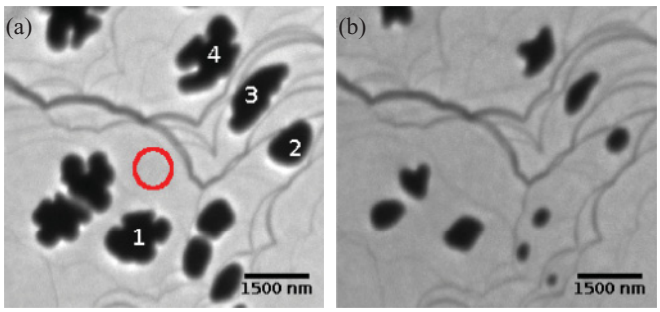

FIG. 12. (Color online) LEEM images of large decaying islands. (a) At the start of the experiment at $T = 375$ K. The circle marks the area used to measure the mean density. (b) At the end of the experiment at $T = 400$ K. The contrast change of the Cu terraces shows the increased BDA density.

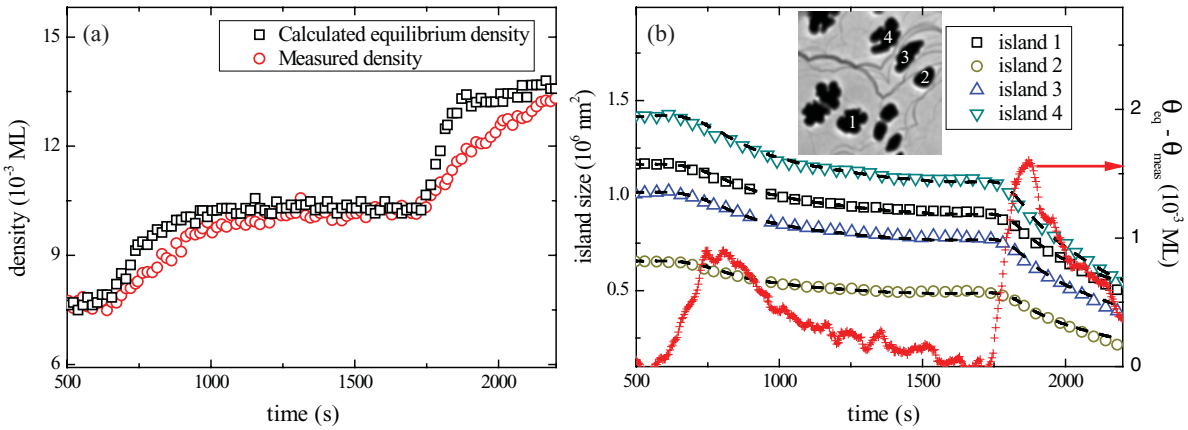

FIG. 13. (Color online) (a) Measured density surrounding the islands from Fig. 12 (red circles) and equilibrium density (black squares) calculated with the help of the phase diagram (Fig. 7). The temperature is raised in a first swift step at 600 s from 375 to 386 K and then in a second swift step at 1740 s to 400 K. The sharp change at $t = 1800$ s is due to a reduced heating power. (b) Measured island size as a function of time together with the fitted curves (dashed lines). The small red pluses show the difference between the two curves in (a). This curve is used as the driving force for the island decay.

Unlike for the small islands, we will now use Eq. (7) directly. We know θ_r from the sample temperature and we can measure $\overline{\theta}$. Despite the cauliflower shape, the islands' curvatures are very small and we can replace θ_r with θ_∞ without introducing a large error. The decay rate should thus simply be given by the difference of $\overline{\theta}$ and θ_∞.

In Fig. 13 (a), we show both $\overline{\theta}$ and θ_∞. The temperature was first increased at $t = 600$ s, then a second time at $t = 1740$ s. After each step, the temperature was kept constant at the new value. θ_∞ has been calculated following exactly the actual variation of the temperature. The difference of the two curves is plotted in Fig. 13(b). This curve was used to fit the decay of four islands, which is shown in the same graph.

We can describe the decay of all four islands by taking the difference between $\overline{\theta}$ and θ_∞ multiplied with a constant value (κ) as the decay rate. The value of κ is different from island to island and was used as a fit parameter. The last part could not be fitted, probably because the assumption of a constant screening length starts to fail. The shape and the local geometry are changing too much. The unknown parameters in κ are the temperature dependent diffusion constant $D(T) = D_0 \exp(\frac{-E_D}{kT})$ and the screening length l_c. Unfortunately, the temperature difference is too small to get a meaningful value for the diffusion barrier E_D. We could fit the data with values ranging from 0 to 0.6 eV, however slightly better fits are obtained with a diffusion barrier in the middle of that range. We find that κ depends almost linearly on the initial island size and has values between 2.5×10^4 nm^2 s^{-1} (island 2) and 4.75×10^4 nm^2 s^{-1} (island 4). The reason for this is a size-dependent screening length l_c. It is impossible to give an analytic expression for the screening length. However, ignoring the complex shapes and using the exact expression for a concentric geometry, $l_c = \ln(\frac{r+R}{r})$, it is obvious that l_c will decrease for increasing island size, as long as R is a constant. Surprisingly, κ seems to be almost independent of the islands' surroundings. For instance, the fits for islands 1 and 3 result in almost the same κ ($\approx 3.4 \times 10^4$ nm^2 s^{-1}), but their environment is substantially different. While island 3 is blocked by Cu steps on two sides and is located on a small terrace, island 1 is situated on a large terrace and is relatively open to all sides. Apparently, Cu steps are not limiting the diffusion of molecules, since otherwise a smaller κ (i.e., a slower decay) would be expected for the island located on a smaller terrace.

VI. DISCUSSION ON ISLAND DECAY

We analyzed the decay of single BDA domains using two methods. First we studied the decay of small islands at 362 K using a classical Ostwald ripening approach. Except for the screening length l_c, we have all ingredients to calculate the diffusion constant D from the fitted prefactors ($\alpha = 400$ nm^2 s$^{-2/3}$). However, we can estimate l_c using the exact expression for a concentric geometry. Since we cannot observe density gradients between the islands, the equilibrium density has to be reached close to the islands' edges, probably within a few tens of nanometers. This would result in $l_c \approx 0.5, \ldots, 1$ and a diffusion constant in the range of 850–1700 nm^2 s^{-1} at 362 K.

In order to avoid the local correlations during the decay process, we also analyzed the decay of larger, further separated islands and used the difference between θ_∞ and measured $\overline{\theta}$ surrounding the islands as the driving force for decay. Using this single curve, we could fit the decay of four islands, each with an individual, size-dependent rate constant κ. The decay rate is independent of the island's location on the underlying Cu substrate. This means that BDA diffusion is not limited by Cu steps. It is important to note that this observation is independent of the model used, i.e., whether the decay is limited by diffusion or by detachment of molecules. It is solely based on the observation of comparable decay rates for islands having completely different relations to step edges. Another observation showing the transparency of steps for BDA diffusion is that terraces which are free of BDA islands follow the same contrast change as the other terraces upon changing the substrate temperature. If there was a significant barrier for molecules to cross, there should be a delay during which the densities on the terraces equilibrate.

As for the small islands in Fig. 11, we cannot resolve BDA density gradients, which implies that the density falls off rather fast from BDA island edges. Assuming that within 100 nm from the islands' edge the mean density is reached, we find $l_c = \ln(\frac{100\ \text{nm}+r}{r}) = 0.14, \ldots, 0.22$, depending on island size r. With these numbers we can give a further estimate for the diffusion constant: $1050 \pm 100\ \text{nm}^2\,\text{s}^{-1}$ in the temperature range between 375 and 400 K. This value is an estimate that is relying on the assumption of diffusion limited decay. As we already mentioned, we cannot exclude a mixed case, in which the detachment rate of molecules also influences the decay.

Another way to measure diffusion constants of organic molecules on a surface is by STM, either at low temperature when the diffusion is slow enough to observe single hopping of molecules[42] or by placing the tip over the surface and measuring the fluctuations of the tunneling current.[43] In the latter reference, again for PTCDA on Ag(100), a diffusion constant of $(4 \pm 1.1) \times 10^3\ \text{nm}^2\,\text{s}^{-1}$ was found at room temperature.

The tracer diffusion constant is measured by STM. This constant refers to the rate at which individual molecules hop between lattice sites, which at low coverages is given through an attempt frequency and a Boltzmann factor containing the diffusion barrier.[44,45] Here we determined the chemical diffusion constant, which describes the rate at which density gradients equilibrate following Fick's law. To be precise, we used the density gradients from the islands' edges to the area farther away where the mean density is reached. Individual molecules still hop in a random way from site to site, going with almost equal chance toward or away from the island edge, but there is still a net mass flow away from the islands.

The high coverage in the dilute phase relative to the crystalline phase will lead to strong molecular interaction, changing the diffusion constant in different directions:[46] Blocking of lattice sites, attractive interaction through hydrogen bonds, and repulsive forces from the negatively charged carboxylate groups will make both the tracer and chemical diffusion constant a complex function of coverage and temperature. One could even imagine a situation in which, due to a larger equilibrium density, the diffusion constant at a higher temperature is smaller than at a lower temperature.

VII. CONCLUSIONS

We studied the temperature dependent equilibrium density of the dilute phase formed by BDA molecules surrounding ordered hydrogen bonded BDA networks with LEEM by measuring the local electron reflectivity. The amount of molecules in the dilute phase is substantial, with densities of up to 30% of the crystalline phase. We analyzed the resulting 2D phase diagram with a lattice gas model and found a cohesive energy of $E_C = 0.35 \pm 0.03$ eV. This value also contains a coverage-dependent interaction term, which we cannot separate from the cohesive energy using our data. However, we can estimate the interaction term to be small, if compared with E_C. We also see large entropy effects, originating from the large size and structure of the BDA molecules. These entropy effects lead to a large density in the dilute phase relative to the crystalline phase. From the cohesive energy, it follows that an individual hydrogen bond has a strength of approximately 0.09 eV, a value which is typical for this type of bond.

We also studied the decay behavior of individual BDA domains, and we found indications for diffusion limited decay, although no pure case could be made. By applying a classic Ostwald ripening model to a set of smaller domains, we can estimate the diffusion constant at 362 K to be between 850 and $1700\ \text{nm}^2\,\text{s}^{-1}$. However, local correlations, characteristic for (partial) diffusion limited decay, have a large influence on the decay behavior of individual islands. To avoid these effects, we also studied the decay of larger, more separated domains. We modeled the decay using the difference between measured density and equilibrium density as the driving force. In the temperature range of 375–400 K, we estimate the diffusion constant to be $1050 \pm 100\ \text{nm}^2\,\text{s}^{-1}$. The decay is independent of the underlying Cu substrate's topography: domains located on a small Cu terrace decay the same way as domains on a larger terrace. This means that Cu steps do not act as high barriers for BDA diffusion.

[1] J. V. Barth, J. Weckesser, C. Cai, P. Günter, L. Bürgi, O. Jeandupeux, and K. Kern, Angew. Chem. Int. Ed. **39**, 1230 (2000).
[2] J. K. Gimzewski, Science **283**, 1683 (1999).
[3] D. Philp and J. F. Stoddart, Angew. Chem. Int. Ed. **35**, 1154 (1996).
[4] G. Whitesides, J. Mathias, and C. Seto, Science **254**, 1312 (1991).
[5] N. Lin, A. Dmitriev, J. Weckesser, J. V. Barth, and K. Kern, Angew. Chem. Int. Ed. **41**, 4779 (2002).
[6] C. Perry, S. Haq, B. G. Frederick, and N. V. Richardson, Surf. Sci. **409**, 512 (1998).
[7] S. Stepanow, T. Strunskus, M. Lingenfelder, A. Dmitriev, H. Spillmann, N. Lin, J. V. Barth, C. Wöll, and K. Kern, J. Phys. Chem. B **108**, 19392 (2004).
[8] S. Stepanow, N. Lin, F. Vidal, A. Landa, M. Ruben, J. V. Barth, and K. Kern, Nano Lett. **5**, 901 (2005).
[9] F. S. Khokhar, R. van Gastel, D. Schwarz, H. J. W. Zandvliet, and B. Poelsema, J. Chem. Phys. **135**, 124706 (2011).
[10] N. Zhu, T. Osada, and T. Komeda, Surf. Sci. **601**, 1789 (2007).
[11] M. Ruben, D. Payer, A. Landa, A. Comisso, C. Gattinoni, N. Lin, J.-P. Collin, J.-P. Sauvage, A. De Vita, and K. Kern, J. Am. Chem. Soc. **128**, 15644 (2006).
[12] F. S. Khokhar, R. van Gastel, and B. Poelsema, Phys. Rev. B **82**, 205409 (2010).
[13] U. Linke and B. Poelsema, J. Phys. E **18**, 26 (1985).
[14] R. Bouwman, J. Vac. Sci. Technol. **15**, 91 (1978).
[15] B. Poelsema, L. K. Verheij, and G. Comsa, Surf. Sci. **152-153**, 851 (1985).
[16] B. Poelsema, S. T. de Zwart, and G. Comsa, Phys. Rev. Lett. **51**, 522 (1983).
[17] B. Poelsema, L. K. Verheij, and G. Comsa, Phys. Rev. Lett. **51**, 2410 (1983).
[18] B. Poelsema, L. K. Verheij, and G. Comsa, Phys. Rev. Lett. **49**, 1731 (1982).

[19]J. de la Figuera, N. C. Bartelt, and K. McCarty, Surf. Sci. **600**, 4062 (2006).
[20]E. Loginova, N. C. Bartelt, P. J. Feibelman, and K. F. McCarty, New J. Phys. **11**, 063046 (2009).
[21]E. Loginova, N. C. Bartelt, P. J. Feibelman, and K. F. McCarty, New J. Phys. **10**, 093026 (2008).
[22]I. V. Markov, *Crystal Growth For Beginners*, 2nd ed. (World Scientific, Singapore, 2003), Chap. 2.1 .
[23]M. J. Sparnaay, Surf. Sci. Rep. **4**, 101 (1985).
[24]A. Dmitriev, N. Lin, J. Weckesser, J. V. Barth, and K. Kern, J. Phys. Chem. B **106**, 6907 (2002).
[25]A. Bilić, J. R. Reimers, N. S. Hush, R. C. Hoft, and M. J. Ford, J. Chem. Theor. Comput. **2**, 1093 (2006).
[26]H. Ibach, *Physics of Surfaces and Interfaces*, 1st ed. (Springer, Berlin, Heidelberg, New York, 2006).
[27]J. A. Venables, *Introduction to Surface and Thin Film Processes* (Cambridge University Press, Cambridge, 2000).
[28]S. Berner, M. Brunner, L. Ramoino, H. Suzuki, H.-J. Güntherodt, and T. A. Jung, Chem. Phys. Lett. **348**, 175 (2001).
[29]J. Ikonomov, C. H. Schmitz, and M. Sokolowski, Phys. Rev. B **81**, 195428 (2010).
[30]T. Steiner, Angew. Chem. Int. Ed. **41**, 49 (2002).
[31]G. Schulze Icking-Konert, Surf. Sci. **398**, 37 (1998).
[32]K. Morgenstern, Surf. Sci. **441**, 289 (1999).
[33]K. Morgenstern, G. Rosenfeld, and G. Comsa, Phys. Rev. Lett. **76**, 2113 (1996).
[34]G. Rosenfeld, K. Morgenstern, I. Beckmann, W. Wulfhekel, E. Laegsgaard, F. Besenbacher, and G. Comsa, Surf. Sci. **402–404**, 401 (1998).
[35]W. Theis, N. C. Bartelt, and R. M. Tromp, Phys. Rev. Lett. **75**, 3328 (1995).
[36]H. Hibino, C. W. Hu, T. Ogino, and I. S. T. Tsong, Phys. Rev. B **63**, 245402 (2001).
[37]Q. Zheng and J. D. Gunton, Phys. Rev. A **39**, 4848 (1989).
[38]M. Giesen, Prog. Surf. Sci. **68**, 1 (2001).
[39]P. A. Thiel, M. Shen, D.-J. Liu, and J. W. Evans, J. Phys. Chem. C **113**, 5047 (2009).
[40]I. Lifshitz and V. Slyozov, J. Phys. Chem. Solids **19**, 35 (1961).
[41]B. Gilbert, R. Andres, P. Perfetti, G. Margaritondo, G. Rempfer, and G. De Stasio, Ultramicroscopy **83**, 129 (2000).
[42]J. Weckesser, J. V. Barth, and K. Kern, J. Chem. Phys. **110**, 5351 (1999).
[43]J. Ikonomov, P. Bach, R. Merkel, and M. Sokolowski, Phys. Rev. B **81**, 161412 (2010).
[44]R. Gomer, Rep. Prog. Phys **53**, 917 (1990).
[45]G. L. Kellog, Surf. Sci. Rep. **21**, 1 (1994).
[46]E. C. Viljoen and C. Uebing, Langmuir **13**, 1001 (1997).